Published in final edited form as:
Anal Chem. 2009 November 1; 81(21): 8758–8764. doi:10.1021/ac901028b.

Lipid Profiles of Canine Invasive Transitional Cell Carcinoma of the Urinary Bladder and Adjacent Normal Tissue by Desorption Electrospray Ionization Imaging Mass Spectrometry

Allison L. Dill[1], **Demian R. Ifa**[1], **Nicholas E. Manicke**[1], **Anthony B. Costa**[1], **José A. Ramos-Vara**[3], **Deborah W. Knapp**[2,4], and **R. Graham Cooks**[1,*]

[1]Department of Chemistry and Center for Analytical Instrumentation Development, Purdue University, West Lafayette, IN 47907, USA

[2]Department of Veterinary Clinical Sciences, Purdue University, West Lafayette, IN 47907, USA

[3]Department of Comparative Pathobiology, Purdue University, West Lafayette, IN 47907, USA

[4]Purdue Cancer Center, Purdue University, West Lafayette, IN 47907, USA

Abstract

Desorption electrospray ionization (DESI) mass spectrometry (MS) was used in an imaging mode to interrogate the lipid profiles of thin tissue sections of canine spontaneous invasive transitional cell carcinoma (TCC) of the urinary bladder (a model of human invasive bladder cancer) as well as adjacent normal tissue from four different dogs. The glycerophospholipids and sphingolipids that appear as intense signals in both the negative ion and positive ion modes were identified by tandem mass spectrometry (MS/MS) product ion scans using collision-induced dissociation. Differences in the relative distributions of the lipid species were present between the tumor and adjacent normal tissue in both the negative and positive ion modes. DESI-MS images showing the spatial distributions of particular glycerophospholipids, sphinoglipids and free fatty acids in both the negative and positive ion modes were compared to serial tissue sections that were stained with hematoxylin and eosin (H&E). Increased absolute and relative intensities for at least five different glycerophospholipids and three free fatty acids in the negative ion mode and at least four different lipid species in the positive ion mode were seen in the tumor region of the samples in all four dogs. In addition, one sphingolipid species exhibited increased signal intensity in the positive ion mode in normal tissue relative to the diseased tissue. Principal component analysis (PCA) was also used to generate unsupervised statistical images from the negative ion mode data and these images are in excellent agreement with the DESI images obtained from the selected ions and also the H&E stained tissue

Keywords

ambient ionization; bladder cancer; imaging; lipidomics; mass spectrometry

*Corresponding Author Professor R. Graham Cooks, Department of Chemistry, Purdue University, West Lafayette, IN, 47907, Tel: (765) 494-5262, Fax: (765) 494-9421, cooks@purdue.edu.

Supporting Information negative ion mode full scan mass spectra of bladder tissue of a healthy dog, and adjacent normal bladder tissue of dog 4. Negative ion mode full scan mass spectrum of dog tumor bladder tissue from m/z 770 to m/z 900. Negative ion mode full-scan mass spectra of dog tumor bladder tissue of dogs 1, 2, 3, and 4. Negative ion mode tissue imaging of normal and cancer regions of bladder tissue of dogs 1, 3, and 4. Principal component analysis loading plot for dog 2

Introduction

Many challenges are still to be met in the diagnosis and management of cancer. These include development of methods for rapid diagnosis, and the identification of new molecular targets for detection, diagnosis, and therapy and, ultimately, the ability to distinguish diseased from non-neoplastic tissues *in vivo* or at least intra-operatively, Lipids represent a diverse group of biomolecules which may provide valuable information to help address these challenges.

Lipids play many different roles in cellular processes both in animals and plants. It is known that the lipid composition of plant species change in response to physical and environmental stress.[1, 2] It has been reported that alterations in the glycerophospholipid composition of tissues occur in certain diseases, including cancer and Alzheimer's disease.[3–6] For example, particular glycerophospholipids and their enzymatic by-products have been identified in malignant transformations in tissue.[7, 8] In another case, the expression of phosphatidylserine in the outer leaflet of the membrane has been found to play a role in the recognition of altered cells, such as cancer cells, by macrophages that can then destroy these cells.[9–11] Lipids are also useful marker compounds of the biological processes involved in cardiovascular diseases, including atherosclerosis.[12, 13] These findings highlight the importance of determining the lipid composition of biological tissue for potential disease detection. There is also evidence to support the need for comprehensive lipidome analysis in order to determine the cascading effects that environmental and other changes have on the presence and amounts of individual lipid species.[14] As an example, shotgun lipidomics has been used to determine the absolute abundances of over 250 different lipids species, covering approximately 95% of the yeast lipidome of *Saccharomyces cerevisiae*.[14] As a result of this comprehensive analysis, it was possible to demonstrate that differences in growth temperature and defects in the lipid biosynthesis pathways resulted in alterations that could be seen throughout the entire yeast lipidome.[14]

Imaging mass spectrometry combines the chemical information collected for multiple analytes using the mass spectrometer with spatial information; this makes it a useful tool for analyzing histological sections of biological tissue.[15–17] DESI,[18] a newer methods of implementing MS imaging,[19] is much less well known than matrix-assisted desorption ionization (MALDI) imaging and SIMS imaging. It uses the standard microprobe imaging procedure, which in this case involves moving the probe spray continuously across the surface while recording mass spectra. Each pixel yields a mass spectrum, which can then be compiled to create an image showing the spatial distribution of particular compounds. Such an image allows one to visualize the differences in the distribution of particular compounds over the tissue section. If independent information on biological properties of the tissue is available, then the MS spatial distribution can provide chemical correlations with biological function or morphology. The spatial resolution of DESI is relatively low, typically 150–250 μm,[20] although spot sizes as small as 40 μm have recently been reported under optimized conditions.[21] The advantage of the method is that the experiment is done in the ambient environment, without chemical pretreatment of the tissue section. Imaging mass spectrometry has developed rapidly in the past decade[17, 22] and has the potential to be a complementary method for analyzing histological sections of biological tissue, because it can provide detailed information about the particular molecular species present in the tissue sample.

Canine spontaneous invasive transitional cell carcinoma (TCC) of the bladder is similar to human bladder cancer with respect to histopathologic characteristics, molecular features, biological behavior such as metastasis, response to medical therapy, and prognosis.[23] There are also differences between canine and human TCC, including differences in gender predilection and the location of the TCC within the bladder.[23] The similarities make canine

TCC a relevant animal model of human invasive bladder cancer, and promising results of dog studies have resulted in advances in human TCC treatment.[23, 24]

Dog bladder cancer tissue sections and adjacent normal tissues were imaged using DESI mass spectrometry. Cancerous and non-cancerous tissues were diagnosed by histological examination of H&E stained sections. Adjacent tissue (sometimes a single section, sometimes several adjacent sections) were imaged with DESI-MS, and the cancerous and non-cancerous tissues were examined in order to determine if differences were present in the lipid profiles as determined by mass spectrometry. Glycerophospholipids (GPs) and sphingolipids (SM) are readily observed species in the DESI mass spectra of dog bladder tissue samples and the study will therefore focus on these lipids. The imaging mass spectrometry data were subjected to multivariate statistical analysis using principal component analysis (PCA) in order to determine if the results correlated with those obtained from H&E staining and with DESI-MS images of particular selected lipids. The aim was to determine if cancerous and non-cancerous tissues for canine TCC could be distinguished using imaging mass spectrometry with an unsupervised statistical method, and whether DESI lipid imaging mass spectrometry has the potential to serve as a tool for future cancer detection and diagnosis in humans.

Experimental

Canine Tissues Studied

Collection of tissues was done following the guidelines and approval of the Purdue Animal Care and Use Committee and with informed dog owner consent. Tissues were obtained from dogs with naturally-occurring TCC who were undergoing evaluation and treatment at the Purdue University Veterinary Teaching Hospital. Tissues were obtained in two settings. For dogs undergoing surgical resection of their bladder tumor as part of their treatment, a section of the tissue specimen containing TCC and adjacent normal was obtained for MS analysis. For dogs that were euthanized at the request of their owner (due to poor quality of life related to the cancer or other conditions), permission to perform a necropsy was obtained, and bladder tissues collected post mortem. In addition to bladder samples, in one case, samples from a cutaneous TCC metastasis along with adjacent normal skin were collected (dog 1).

Tissue Preparation

All fresh tissue samples were flash frozen in liquid nitrogen and subsequently stored in closed containers at −80°C. The tissue sampled included two matched pairs, one piece of tumor tissue and a separate piece of adjacent normal-appearing bladder tissue, from different dogs (dog 1 and dog 2), along with two pieces of tissue from different dogs (dog 3 and dog 4) containing both tumor and adjacent normal tissue in one tissue piece. The tissue samples were sliced into 15 micrometer thick sections using a Shandon SME cryotomoe cryostat (GMI, Inc., Ramsey, MN, USA) and thaw mounted onto glass slides. The tissue sections were individually sliced and mounted by hand onto the glass slides, with the result that the tissue orientation on each slide was slightly different. H&E stained images were rotated to match the orientation of the DESI-MS images. The tissue sections mounted onto the glass slides were stored in closed containers at −80°C until analysis. The tissue sections were allowed to come to room temperature and then dried under nitrogen in a dessicator overnight prior to analysis.

Mass Spectrometry

The DESI ion source used was a lab-built prototype, configured as described previously.[25] The DESI spray was positioned 2 mm from the tissue surface at an incident angle of 52° (to the sample surface) and a low (ca 10°) collection angle was used for all of the experiments discussed. The spray solvent for MS acquisition in the negative and positive ion modes was acetonitrile:water (50:50) with a 5 kV spray voltage applied. Acetonitrile was purchased from

Sigma-Alrich (St. Louis, MO, USA) and water (18.2 MΩ-cm) was from a PureLab ultra system by Elga LabWater (High Wycombe, UK). The nitrogen gas pressure was 100 psi and the solvent flow rate was 1.5 μL/min. In the tissue imaging experiments, the tissue was scanned using a 2D moving stage in horizontal rows separated by a 250 μm vertical step until the entire tissue sample was assayed.[20] All experiments were conducted using a LTQ linear ion trap mass spectrometer controlled by XCalibur 2.0 software (Thermo Fisher Scientific, San Jose, CA, USA). An in-house program allowed the conversion of the XCalibur 2.0 raw files into a format compatible with the BioMap (freeware, http://www.maldi-msi.org) software. The individual spectra or pixels that were acquired were assembled into a spatially accurate image using the BIOMAP software.

PCA Analysis

Data were processed in Matlab 2008a, The MathWorks (Natick, MA, USA). Each pixel includes a full mass spectrum covering the full mass range recorded in the original data. All pixels were normalized by calculating the median area under the curve for the full image and scaling each pixel to this value. No background adjustment or smoothing filters were necessary. Principal component analysis (PCA) was performed on each entire image. Principal component eigenvalues and eigenvectors were ordered in terms of decreasing component variance. Only the first 3 principal components are used in the data in the present work. Each eigenvalue set corresponding to all pixels for a given principal component (e.g., all eigenvalues calculated for the first principal component eigenvector) were scaled between 0 and 1. For images developed using only one principal component, the eigenvalue set was plotted over the range blue to red (corresponding to 0 and 1, respectively) using the web colors scheme (RGB).

For plots consisting of data from multiple principal components, each eigenvalue set was scaled over the range 0 to 255 and convolved with a hexadecimal value characteristic of a primary color in the web scheme (RGB). That is, PC1 eigenvalues are convolved with red contribution, PC2 with green contribution, and PC3 with blue contribution. A full hexadecimal number is therefore generated for each pixel in the image and is characteristic of the first three principal components. This “web color” was then plotted to create the image.

Loading plots were generated in the standard fashion by plotting PC1 and PC2 score spectra against one another and labeling according to m/z. These plots are a convenient way of extracting information as to which ions (m/z values) are responsible for the majority of the variation in between pixels in a principal component analysis. Individual pixels most responsible for this variation can be immediately identified and compared to false color images of specific ions.

Results and Discussion

Dog bladder tumor tissue and adjacent normal tissue from four different dogs was examined using DESI-MS. In order to optimize the experimental conditions and identify the lipids present, initial experiments was conducted in the line scan mode. Full 2D imaging experiments were conducted in order to examine the spatial distribution of particular lipid species in the different tissue sections and also to produce the unsupervised PCA images. Both the line scan and the specific lipid image data sets were examined for differences in lipid profiles between the tissue sections. The lipid image and PCA image data were compared to the histological data of optical H&E stained images to seek correlations between the chemical and histochemical features of tumor and adjacent normal tissue sections.

Optimization and Identification

Prior to the imaging experiments, the DESI experimental conditions were optimized in order to maximize the signal intensity obtained from the thin tissue sections, in particular for the glycerophospholipid and sphingolipid region of the mass spectrum; this was done separately in both the negative and positive ion modes. Following optimization, a series of line scans was performed across the tumor and adjacent normal tissue samples (or adjacent skin in dog 1 with the cutaneous TCC metastasis), and the resulting mass spectra were examined. It is apparent from the line scans that differences in the mass spectrometric profiles exist between the tumor and adjacent normal tissue types; representative examples are shown for the negative and positive ion modes in Figure 1. Experiments were also conducted on the bladder tissue of a healthy dog, and the mass spectrometric profile is comparable to that of the adjacent normal tissue; a representative spectrum in the negative ion mode for the healthy dog compared to the normal tissue of dog, 4 is shown in Figure S-1.The glycerophospholipid and sphingolipid regions of the spectra exhibit marked differences in the absolute peak intensities between the two tissue regions. The pattern of the relative peak intensities is also different between the tumor and normal spectra in both the negative and positive ion modes. A negative ion mode spectrum showing only the region from m/z 770 to m/z 900 is presented in Figure S-2 in order to show the wealth of information present in the glycerophosplipid region. The differences observed between the spectra of the tissue types were confirmed in three other dogs, with the profiles of the tumor region of the tissue appearing to be similar between the four animals, Figure S-3 shows the negative ion mode spectra for each of the four dogs. These results, found first in the line scan spectra, were confirmed and extended by acquisition of full MS images of the samples.

Collision induced dissociation (CID) tandem MS experiments were conducted to record product ion spectra for peaks detected in the tissue samples. The data were compared to published fragmentation spectra[26–31] in order to identify the particular lipids involved. Because the internal energy deposition in DESI is similar to that in ESI, fragmentation patterns recorded using ion traps in both of these ionization modes could be used for identification.[18, 32]

The principal lipids identified in the negative ion mode are from three lipid classes identified as glycerophosphoserines (PS), glycerophosphoglycerols (PG), and glycerophosphoinositols (PI). The species identified from the dog bladder tissue samples are listed in Table 1.

In the positive ion mode, product ion spectra were recorded from the tissue samples and used in comparison to published fragmentation spectra in the literature allowed positive identification of some of the more intense lipid signals in the full scan mass spectra.[26, 27, 29, 31, 33] Identities can be assigned to several lipid species found in the tissue samples as glycerophosphocholines (PC) and a sphingomyelin (SM). The peak at m/z 782.6 can be identified as the sodium adduct of PC(34:1), m/z 798.5 is the potassium adduct of PC(34:1), m/z 808.6 is the sodium adduct of PC(36:2), and m/z 824.5 is the potassium adduct of PC (36:2). The peak at m/z 741.4 is identified as the potassium adduct of SM(18:1/16:0).

Tissue Imaging using Glycerophospholipid and Sphingolipid Ions

The tissue imaging experiments allow the expansion of the information gained through the line scans as well as the visualization of the results covering the entire tissue sample. All four dog tissue samples were imaged using DESI-MS in both the negative and positive ion modes. Extracted images representing the distribution of ions of one particular m/z value correspond to the distribution of the corresponding molecule (in rare cases, molecules) in the tissue sample. This allows the chemical information obtained from the mass spectrometer to be correlated with the spatial information garnered from the image.

The images of the tissue samples for dog 2 are shown in Figure 2. Along with the selected ion images is an optical image of the sample after histological staining of an adjacent section with H&E. H&E staining allows a pathologist to see the structural details of the tissue sample, but no conclusions can be drawn about the chemical nature of the tissue: the identification of different cell or tissue types are made purely on morphological characteristics. As seen in the images of the tumor tissue, shown on the left of each image, in Figure 2, the tumor tissue exhibits increased absolute intensities for the signals at m/z 788.6, m/z 773.5, m/z 835.7, m/z 863.7 and m/z 786.4 when compared with normal tissue. The peak ratios also show systematic differences, with m/z 773, 835 and 863 being high relative to m/z 788 in the diseased relative to the normal tissue. Following the observations initially made with the DESI data, the H&E stained tissue was used to confirm the tumor diagnosis and to distinguish tumor from adjacent normal sections. The DESI-MS images also allow the detection of abnormal areas in the adjacent tissues that grossly appear to be normal, e.g. detection of some tumor tissue in the adjacent tissue. For example, in dog 2, Figure 2, the tissue adjacent to the tumor mass has a border of tumor tissue in the H&E stained section, shown in dark blue, which correlates to increased signal intensity in the DESI images. It is of interest that this particular observation was first made in the DESI data and then confirmed in the histological examination.

The DESI-MS images for the tumor and adjacent normal tissues samples of dog 1, 3, and 4 are shown in Supporting Figures 4, 5, and 6, respectively. As observed for dog 2, the tumor tissue shows increased molecular anion signals for m/z 788.6, m/z 773.5, m/z 835.7, m/z 863.7 and m/z 786.4, and the areas of increased DESI-MS signal intensity correlate with the portions of tissue diagnosed as tumor by the pathologist. In the H&E stained sections, the tumor tissue is located in the dark blue area, and the normal tissue is present in the pink stained area in each of the Supporting Figures 4, 5 and 6.

Similar images were constructed in the positive ion mode for each dog tissue section based on the masses of lipids of classes PC and SM. Representative images from dog 4 are shown in Figure 3. The PC species at m/z 782.6, m/z 798.5, m/z 808.6 and m/z 824.5 show increased signal intensities in the tumor region of the tissue sample. In the positive ion mode, a compound that correlates inversely with the tumor was also observed. The SM (18:1/16:0) species at m/z 741.5 does not appear in the tumor region of the tissue sample, and only appears in the normal tissue. The images obtained by DESI-MS for the tumor and normal tissue sections in the positive ion mode match the distinctions made by H&E staining of the tissue sections.

Tissue Imaging using Fatty Acid Ions

The previously described images concentrate on the glycerophospholipid and sphingolipid region of the mass spectrum, i.e. from approximately m/z 600 to m/z 1000. However, spectra were collected and images created for the entire mass range from m/z 150 to m/z 1000 for each dog tissue sample. A representative mass spectrum from m/z 150 to m/z 1000 from dog 2 is shown in Figure 4. It shows strong signal intensity in the low mass region corresponding to free fatty acid species. The region from m/z 500 to m/z 650 is most likely comprised of dimers of the free fatty acids of ceramides. DESI-MS images were constructed from three of the intense fatty acid species for each of the four dog samples. A representative series of images for dog 2 is shown in Figure 4, together with the H&E stained image showing the tumor on the left in the dark blue stained area and the normal tissue on the right in the pink stained area. The border of tumor tissue along the bottom of the tissue adjacent to the tumor mass can be seen in the both the DESI-MS images as increased signal intensity and in the H&E stained tissue. These fatty acids can only be tentatively identified since the possibility of isomers must be allowed for; based on the mass of the molecular anion, $[M\text{-}H]^-$; m/z 279.6 is an 18:2 fatty acid ($C_{18}H_{32}O_2$); m/z 281.6 is an 18:1 fatty acid ($C_{18}H_{34}O_2$); m/z 303.5 is a 20:4 fatty acid

($C_{20}H_{32}O_2$). The increased signal intensity seen in the DESI-MS images correlates well with the tumor region of the tissue as identified in the H&E stained images.

PCA Analysis

The dog tumor tissue samples can be distinguished from normal tissue by the images of at least five different lipid species and three fatty acid species in the negative ion mode alone, and at least four different lipid species in the positive mode, representing a potential for a multi-marker strategy for diagnosis. So far the data presented for the multiple images show the intensity of only one ion in each image that was previously selected by the analyst as being of particular interest. The original data was analyzed thoroughly by individual scientists to determine which ions could be used to distinguish between tumor and normal tissue. Principal component analysis (PCA) is an unsupervised statistical method that has been used extensively in analytical chemistry for data dimensionality reduction, post-processing and analysis.[34–37] PCA was run on the entire images simultaneously and eigenvalues associated with each pixel, corresponding to a full mass spectrum, were extracted for each principal component. These values are plotted using the method described in the experimental section, one for each of the first three principal components, together with a 4^{th} image in which each of the three principal components are convolved with a color and plotted in the standard RGB "web color" system. Figure 5 shows the images developed for dog 2. The mixed image gives a simple, unsupervised and general way to visually inspect the data for identification of tumor and normal regions. Visually, marked color differences exist between the tumor tissue on the left in Figure 5 and the normal tissue on the right. These PCA-developed images also display the border of tumor tissue that is present on the bottom edge of the normal tissue that was also detected in the DESI and H&E stained images. We developed a loading plot (Supporting Figure 7) and it shows that the peaks at m/z 788.6, m/z 773.5, m/z 835.7, m/z 863.7 and m/z 786.4 are important signals contributing to the difference between the two tissue types, a fact that correlates well to the results found from manual inspection of selected ion images. The unsupervised statistically generated images for dog 2 are in excellent agreement with the images generated using DESI-MS. These results were confirmed by the H&E staining data.

Reproducibility and Quantitation

Reproducibility is crucial to establishing a potential method for distinguishing between tumor and normal tissue. In this case only four different dog tissue samples from four different dogs were analyzed, a small set but sufficient for initial experiments used to identify trends in the lipid species observed. In addition, at least 5 replicates for each dog sample were prepared and analyzed, with representative images seen in Figure 2–Figure 4 and Supporting Figures 1, 2, 3. In addition, two sections of each sample were subjected to H&E staining and exhibited near-identical results. The DESI-MS imaging method described here for lipid species in dog bladder cancer tissue has been demonstrated to be reproducible across multiple dogs and within multiple samples from the same dog, Supporting Figure S-3 shows the negative ion spectra from all four dogs. The DESI-MS imaging method is also reproducible across both positive and negative ion modes, yielding positive tumor correlations in each polarity.

Conclusion

It has been demonstrated that DESI-MS imaging can distinguish between cancerous and non-cancerous dog bladder tissue samples as well as a cutaneous TCC metastasis sample in the small set of tissue sections examined. Canine bladder cancer is useful for proof of concept experiments, and the resulting methodology can be applied in studies of many other types of cancer, and potentially other disease conditions. The distinction between diseased and healthy tissue was made using multiple marker lipids and multiple free fatty acids in both the positive and negative ion modes for increased confidence in the diagnosis. The glycerophospholipid

and sphingolipid profiles between the tissue types differ, both in the intensities of the lipid signals present and the pattern of the lipid signals. PCA developed images were created providing another level for visualizing the data, and the PCA developed images correlated extremely well to those generated by DESI-MS. Employing a statistical method such as PCA provides the potential for the development of an unsupervised MS imaging technique, in which a sample library can be built and used to classify tissue samples, as cancerous and non-cancerous or to grade the cancers. DESI-MS imaging has the potential for use in a diagnostic capability based on the lipid profiles and intensities found in tissue samples, as shown here for canine TCC samples.

Supplementary Material

Refer to Web version on PubMed Central for supplementary material.

Acknowledgments

We thank Deepika Dhawan, Jane Stewart and Amalia deGortari for their assistance in obtaining all of the dog bladder tissue samples. We thank Stephen Hooser and Grant Burcham for the H&E stained dog tissue samples.

This work was supported by the National Institutes of Health (Grant 1 R21 EB00 9459-01) and Office of Naval Research (Grant N00014-05-1-0454). This work was also supported in part by a fellowship from Merck Research Laboratories.

References

1. Welti R, Shah J, Li WQ, Li MY, Chen JP, Burke JJ, Fauconnier ML, Chapman K, Chye ML, Wang XM. Frontiers in Bioscience 2007;12:2494–2506. [PubMed: 17127258]
2. Wang XM, Li WQ, Li MY, Welti R. Physiologia Plantarum 2006;126:90–96.
3. Athar M. Indian Journal of Experimental Biology 2002;40:656–667. [PubMed: 12587714]
4. Montine TJ, Neely MD, Quinn JF, Beal MF, Markesbery WR, Roberts LJ, Morrow JD. Free Radical Bio Med 2002;33:620–626. [PubMed: 12208348]
5. Sakai K, Okuyama H, Yura J, Takeyama H, Shinagawa N, Tsuruga N, Kato K, Miura K, Kawase K, Tsujimura T, Naruse T, Koike A. Carcinogenesis 1992;13:579–584. [PubMed: 1576710]
6. Shimma S, Sugiura Y, Hayasaka T, Hoshikawa Y, Noda T, Setou M. J. Chromatogr., B: Anal. Technol. Biomed. Life Sci 2007;855:98–103.
7. Aboagye EO, Bhujwalla ZM. Cancer Res 1999;59:80–84. [PubMed: 9892190]
8. Glunde K, Jie C, Bhujwalla ZM. Cancer Res 2004;64:4270–4276. [PubMed: 15205341]
9. Yamaji-Hasegawa A, Tsujimoto M. Biol. Pharm. Bull 2006;29:1547–1553. [PubMed: 16880602]
10. Utsugi T, Schroit AJ, Connor J, Bucana CD, Fidler IJ. Cancer Res 1991;51:3062–3066. [PubMed: 2032247]
11. Zwaal RFA, Comfurius P, Bevers EM. Cell. Mol. Life Sci 2005;62:971–988. [PubMed: 15761668]
12. Pratico D, Iuliano L, Mauriello A, Spagnoli L, Lawson JA, Maclouf J, Violi F, FitzGerald GA. J. Clin. Invest 1997;100:2028–2034. [PubMed: 9329967]
13. Morrow JD. Arterioscler. Thromb. Vasc. Biol 2005;25:279–286. [PubMed: 15591226]
14. Ejsing CS, Sampaio JL, Surendranath V, Duchoslav E, Ekroos K, Klemm RW, Simons K, Shevchenko A. Proc. Natl. Acad. Sci. U. S. A 2009;106:2136–2141. [PubMed: 19174513]
15. Seeley EH, Caprioli RM. Proteomics: Clin. Appl 2008;2:1435–1443.
16. Chaurand P, Cornett DS, Caprioli RM. Curr. Opin. Biotechnol 2006;17:431–436. [PubMed: 16781865]
17. Pacholski ML, Winograd N. Chem. Rev 1999;99:2977. [PubMed: 11749508]
18. Takats Z, Wiseman JM, Gologan B, Cooks RG. Science 2004;306:471–473. [PubMed: 15486296]
19. Wiseman JM, Ifa DR, Song Q, Cooks RG. Angew Chem Int Edit 2006;45:7188–7192.
20. Ifa DR, Wiseman JM, Song QY, Cooks RG. Int J Mass Spectrom 2007;259:8–15.

21. Kertesz V, Van Berkel GJ. Rapid Comm. in Mass Spec 2008;22:2639–2644.
22. Caprioli RM, Farmer TB, Gile J. Anal Chem 1997;69:4751–4760. [PubMed: 9406525]
23. Knapp DW, Glickman NW, DeNicola DB, Bonney PL, Lin TL, Glickman LT. Urologic Oncology 2000;5:47–59.
24. Mutsaers AJ, Widmer WR, Knapp DW. Journal of Veterinary Internal Medicine 2003;17:136–144. [PubMed: 12683611]
25. Manicke NE, Kistler T, Ifa DR, Cooks RG, Ouyang Z. J. Am. Soc. Mass Spectrom 2009;20:321–325. [PubMed: 19013081]
26. Pulfer M, Murphy RC. Mass Spectrometry Reviews 2003;22:332–364. [PubMed: 12949918]
27. Manicke NE, Wiseman JM, Ifa DR, Cooks RG. J. Am. Soc. Mass. Spectrom 2008;19:531–543. [PubMed: 18258448]
28. Hsu FF, Turk J. J. Am. Soc. Mass Spectrom 2000;11:986–999. [PubMed: 11073262]
29. Hsu F-F, Turk J. J. Am. Soc. Mass Spectrom 2008;19:1681–1691. [PubMed: 18771936]
30. Hsu F-F, Turk J. J. Am. Soc. Mass Spectrom 2005;16:1510–1522. [PubMed: 16023863]
31. Murphy, RC. Mass Spectrometry of Lipids. New York: Plenum Press; 1993.
32. Nefliu M, Smith JN, Venter A, Cooks RG. J. Am. Soc. Mass Spectrom 2008;19:420–427. [PubMed: 18187338]
33. Wiseman JM, Puolitaival SM, Takats Z, Cooks RG, Caprioli R. Angew Chem Int Edit 2005;44:7094–7097.
34. Smith PBW, Snyder AP, Harden CS. Anal Chem 1995;67:1824–1830. [PubMed: 9306733]
35. Harrington PD, Voorhees K. J. Anal. Chem 1990;62:729–734.
36. Harrington PD, Street TE, Voorhees KJ, Dibrozolo FR, Odom RW. Anal. Chem 1989;61:715–719.
37. Lindon JC, Holmes E, Nicholson JK. Pharm. Res 2006;23:1075–1088. [PubMed: 16715371]

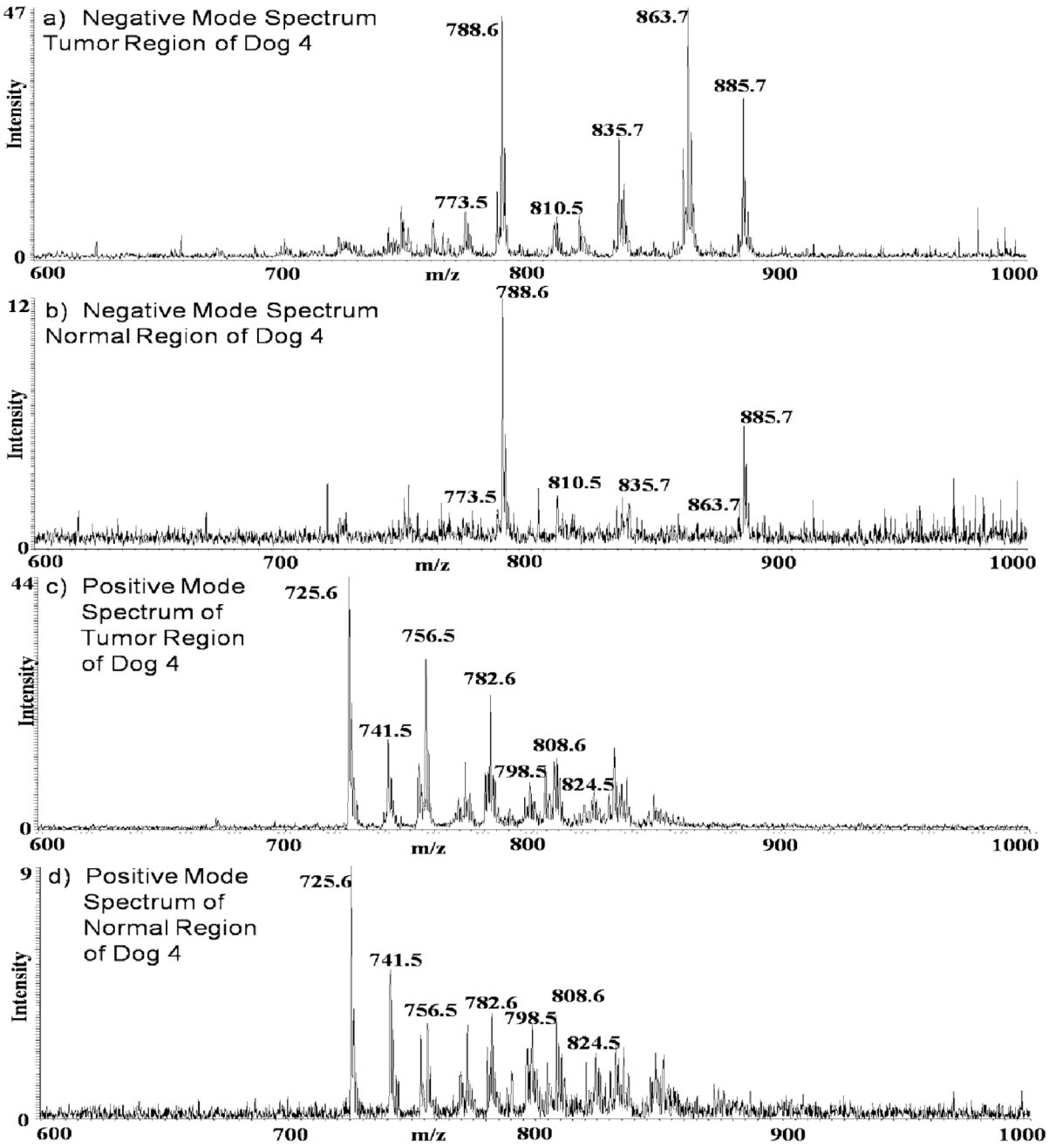

Figure 1.

Typical negative ion mode full scan mass spectra of dog tumor and normal bladder tissue in the range of m/z 600 to m/z 1000. (a) Negative ion mode spectrum of the tumor region of the tissue sample of dog 4. (b) Negative ion mode spectrum of the normal region of the tissue sample of dog 4. (c) Positive ion mode spectrum of the tumor region of the tissue sample of dog 4. (d) Positive ion mode spectrum of the normal region of the tissue sample of dog 4.

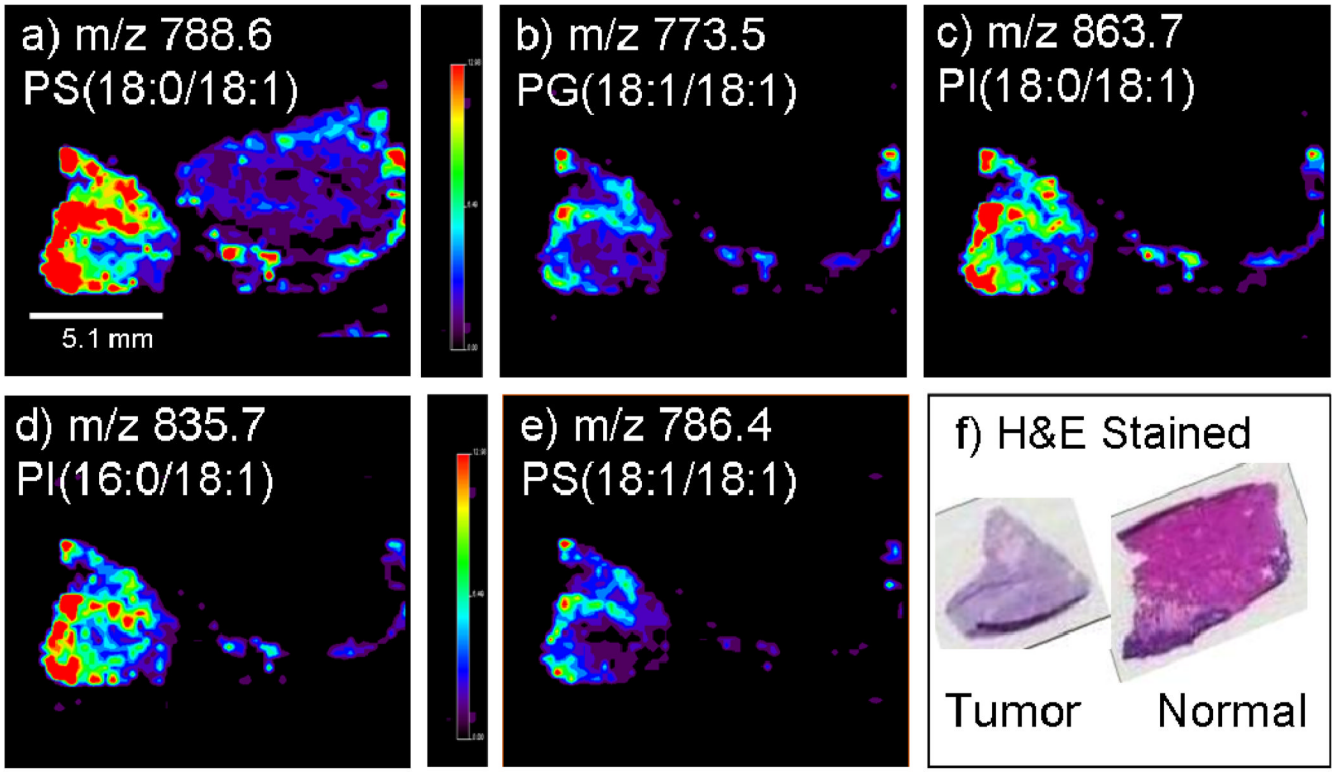

Figure 2.

Negative ion mode tissue imaging of bladder tissues including areas of cancer and adjacent tissues of dog 2; (a) Ion image of m/z 788.6, PC(18:0:18:1) (b) Ion image of m/z 773.5, PG (18:1/18:1) (c) Ion image of m/z 863.7, PI(18:0/18:1) (d) Ion image of m/z 835.7, PI(16:0/18:1) (e) Ion image of m/z 786.4, PS(18:1/18:1) (f) H&E stained tissue sections of the tumor tissue and the tissue adjacent to the tumor. The “tumor” tissue is diffusely infiltrated by transitional cell carcinoma. The “adjacent” tissue (full-thickness bladder specimen) contains tumor cells in the mucosal epithelium (note dark blue stained area on the lower edge of the specimen). The muscularis layer (pink stained area in the middle of the section) and a tissue fold (upper edge of the specimen) are also noted.

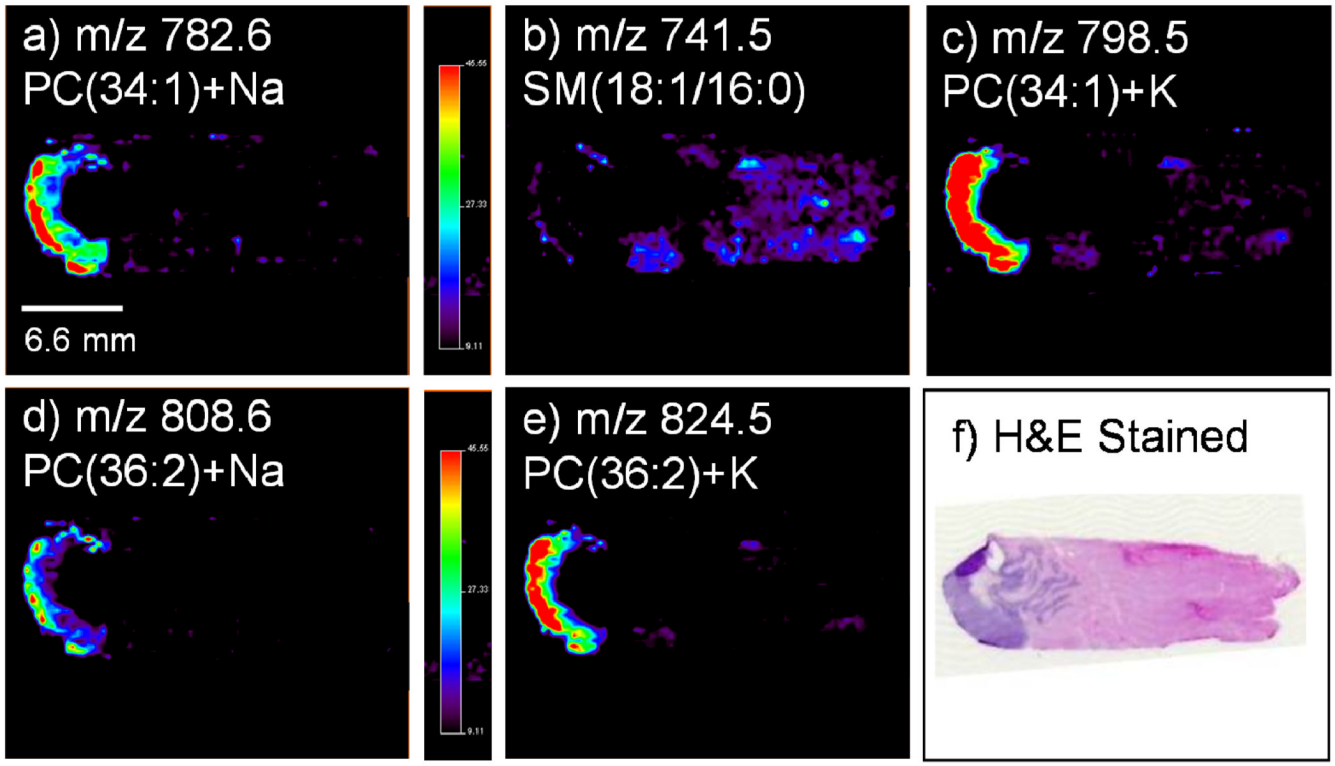

Figure 3.

Positive ion mode tissue imaging of canine urinary bladder with TCC from dog 4; (a) m/z 782.6, PC(34:1)+Na (b) m/z 741.5, SM(18:1/16:0) (c) m/z 798.5, PC(34:1)+K (d) m/z 808.6, PC(36:2)+Na (e) m/z 824.5, PC(36:2)+K (f) H&E stained tissue sections with tumor tissue represented by dark blue color (on left end of the tissue section). The rest of the tissue (pink stained area) is the muscularis of the bladder wall, and no cancer cells are present in this area.

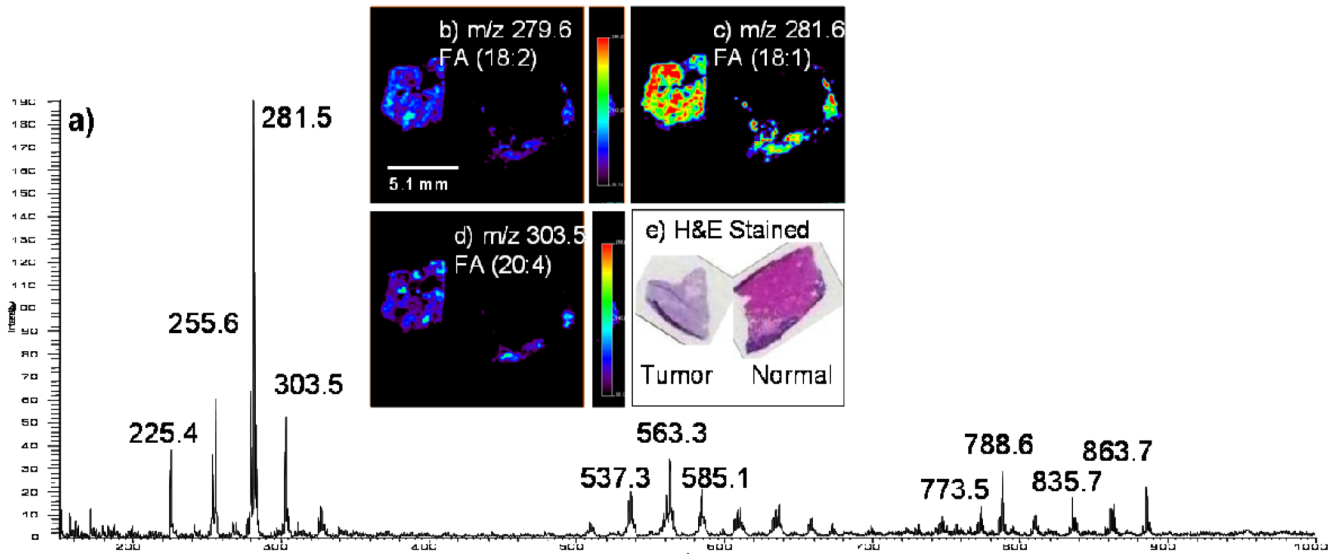

Figure 4.

(a) Negative ion mode full scan spectrum from the tumor region of the tissue sample of dog 2 in the range of m/z 150 to m/z 1000. (b)–(e) Negative ion mode tissue imaging of bladder tissues including areas of cancer and adjacent tissues from dog 2; (b) Ion image of m/z 279.6, fatty acid (18:2) (c) Ion image of m/z 281.6, fatty acid (18:1) (d) Ion image of m/z 303.5, fatty acid (20:4) (e) H&E stained tissue sections of the tumor tissue and the tissue adjacent to the tumor. The "tumor" tissue is diffusely infiltrated by transitional cell carcinoma. The "adjacent" tissue (full-thickness bladder specimen) contains tumor cells in the mucosal epithelium (note dark blue stained area on the lower edge of the specimen). The muscularis layer (pink stained area in the middle of the section) and a tissue fold (upper edge of the specimen) are also noted.

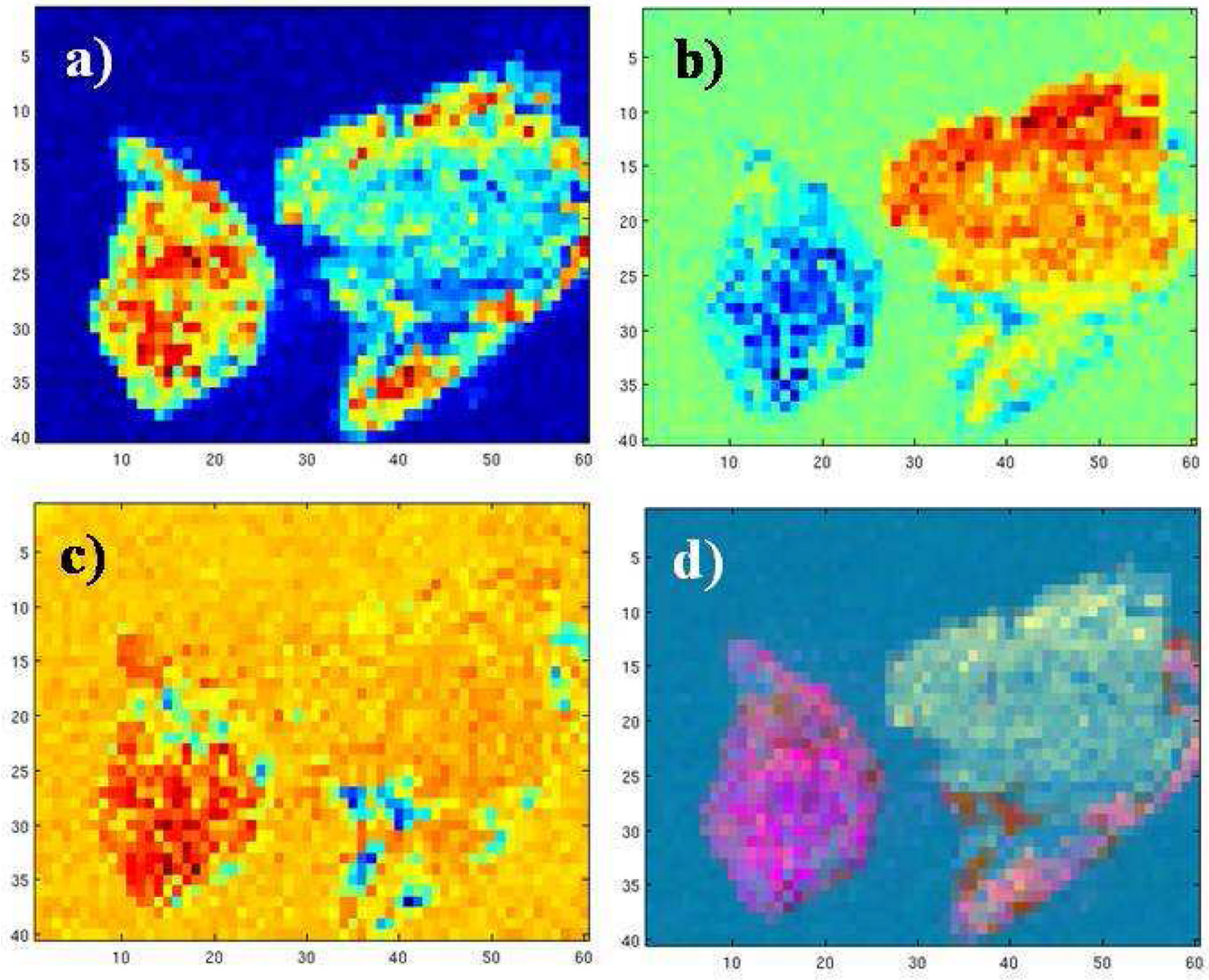

Figure 5.
PCA-developed images of dog 2. **a)** False color plot of PC1 **b)** False color plot of PC2 **c)** False color plot of PC3 **d)** False color plot of PC1, PC2, and PC3.

Table 1

Negative ion mode MS/MS product ion fragmentation pattern of dog bladder tissue.

Peak Identity	Molecular Anion (m/z)	Fragment Anions (m/z)
PS(18:0/18:1)	788.6	283.3, 419.5, 437.5, 701.6
PG(18:1/18:1)	773.5	281.5, 417.3, 491.1
PI(16:0/18:1)	835.7	283.3, 419.9, 553.4, 581.5, 599.6
PI(18:0/18:1)	863.7	283.2, 419.3, 581.3, 599.8
PS(18:1/18:1)	786.4	281.3, 417.3, 437.3, 699.4